



ARTICLE

# Preparation of N,S-Doped Biochar via Modulating Chitosan and Sodium Dodecyl Benzene Sulfonate Interaction and Its Adsorption Performance

Jun-Jie Yang<sup>1</sup>, Ran An<sup>1</sup>, Jing-Heng Nie<sup>1</sup>, Hao-Miao Ma<sup>1</sup>, Yu-Qing Yan<sup>1</sup>, Yuan-Ru Guo<sup>1,\*</sup> and Qing-Jiang Pan<sup>2,\*</sup>

<sup>1</sup>Key Laboratory of Bio-based Material Science & Technology (Ministry of Education), College of Material Science and Engineering, Northeast Forestry University, Harbin, 150040, China

<sup>2</sup>Key Laboratory of Functional Inorganic Material Chemistry (Ministry of Education), School of Chemistry and Materials Science, Heilongjiang University, Harbin, 150080, China

\*Corresponding Authors: Yuan-Ru Guo. Email: guoyrnefu@163.com; Qing-Jiang Pan. Email: panqjitc@163.com

Received: 19 December 2024; Accepted: 25 February 2025; Published: 20 May 2025

**ABSTRACT:** To achieve the sustainable development and carbon neutral target, biomass chitosan (CS) was used to prepare N,S-doped biochar (NSB) with the assistance of sodium dodecyl benzene sulfonate (SDBS). The synthetic route was developed, which does not require the activation that is frequently-used for active carbon materials. By manipulating their interaction, SDBS was deposited with CS in neutral and basic conditions. Subsequent calcination successfully has access to NSB. It features with hierarchical porous structure and abundant functional groups. The dually-doped NSB bears excellent adsorption performance towards chlortetracycline (CTC). The adsorption capacity reaches 101.3 mg g<sup>-1</sup> within 4 h. It is 200% higher than that of N-doped biochar (NB) prepared by only CS. The renewable and cost-effective raw materials and simple preparation method would enable NSB to be a good candidate for remedying antibiotics in the environment.

**KEYWORDS:** Biomaterial; element-doped biochar; interfacial interaction; chlortetracycline

## 1 Introduction

Broad-spectrum antibiotics were widely used to treat bacterial and fungal infections since they could inhibit the protein synthesis of bacteria. Of them, tetracycline is one of the most prevalent and important antibiotic drugs. It is massively consumed every year. The annual usage is as high as 11,200 t [1–3]. Residues of antibiotics from medical and livestock wastewater cause serious pollution in the natural environment [4,5]. They disrupt the necessary microbial community structure and threaten the safety of the ecological environment.

Many approaches have been applied to solve these problems, such as photocatalytic degradation, biodegradation, electrochemical treatment, etc. [6–10]. The photocatalytic degradation is operated under mild conditions and greatly mineralizes the concentrations of antibiotics. However, photocatalysts are usually prone to low efficiency and high preparation costs. Biodegradation is an ecofriendly and energy-efficient method, but microorganisms need long acclimation and are also sensitive to the environment. Electrochemical treatment offers rapid degradation of antibiotics in a highly efficient way. However, it suffers from high energy demand, side reactions as well as safety risks, restricting further applications [11].



So far, adsorption is believed to be one of the most effective ways of removing tetracycline antibiotics from polluted water. Carbon materials have been widely used for sewage treatment. They have the advantages of simple operation, high adsorption efficiency, low energy consumption and sustainable use [12–16]. Many sorts have been paid attention to, including active carbons, graphene and chars [17–19]. For example, graphene and oxidized ones have chronic toxicity [20,21], which would affect the diversity of microbial communities. Environmentally-friendly active carbon was considered as a good candidate. However, it would require activation for adsorption use and risk environmental pollution [22,23]. This also raised energy consumption. Thus, it is still highly demanding to seek a green way to prepare carbon materials [24,25].

Biochar [26–28] is a type of carbon material. It is obtained by pyrolysis of biomass under anaerobic or low oxygen atmosphere conditions. As a cost-effective carbon material, biochar has physicochemical properties similar to activated carbon materials [29,30]. Briefly, biochar can show good properties even without activation. This offers it a good prospect to work as an adsorbent [31–33]. At the same time, most biochar materials have abundant oxo functional groups, like carboxyl and phenolic hydroxyl [34–36]. These allow biochar to easily interact with antibiotics and organic aromatic pollutants, through  $\pi$ - $\pi$  electron donor acceptor interaction (EDA), electrostatic attraction, hydrogen bonding, etc. [37].

A lot of biomaterials, such as cellulose, lignin, wood and straw, have been reported for preparing biochar [38]. Chitosan (CS) is a natural nitrogen-containing biomass material and composed of  $\beta$ -(1,4)-N-acetyl-d-glucosamine units [39–41]. It is extracted from by-products like shrimp and crab shells in seafood processing engineering and obtained through deacetylation [42]. CS can directly synthesize nitrogen-doped biochar (NB) without adding any other nitrogen source chemicals. Chen et al. [43] prepared CS-FeS biochar composite materials by using CS as a carbon source. In removing heavy metal uranium (VI) from wastewater, the equilibrium adsorption capacity reaches  $92.45 \text{ mg g}^{-1}$  at room temperature. Previous studies showed that CS-derived biochar had relatively good adsorption properties, but its low specific surface area and low pore volume still limited the performance. How to tune the structure of CS-derived biochar is becoming critical in the respect.

As a weak polyelectrolyte, CS can dissolve in water and form cations in the acidic solution. It would produce the polyelectrolyte complex (PEC) by combining with anionic polyelectrolyte. Inspired by this, SDBS [44,45] was used to assemble with CS in this work. SDBS is long chain surfactant and carries negative charges in water. It would form PEC with positively charged CS via electrostatic attraction, hydrogen bonding and hydrophobic interactions. At the same time, SDBS has sulfonic acid groups, which could introduce the S element into biochar after calcination. This would enrich the types of functional groups as well as active sites on the sample surface, and thus improve the adsorption performance. Then the N and S-doped biochar (NSB) was prepared. The calcination was performed only once. No activation and the second calcination process were needed. The treatment of CTC in water was fully studied. The adsorption mechanism was also addressed by different adsorption models.

## 2 Materials and Methods

### 2.1 Materials

The CS (food grade) was purchased from Shandong Luhai Lansheng Biotechnology Co., Ltd., Dongying, China. SDBS, sodium hydroxide, glacial acetic acid, and hydrochloric acid were purchased from Tianjin Kemio Chemical Reagent Co., Ltd., Tianjin, China. Anhydrous ethanol was purchased from Tianjin Fuyu Fine Chemical Reagent Factory. Chlortetracycline hydrochloride (CTC) was purchased from Jiangxi Zhenghe Biotechnology Co., Ltd., Nanchang, China.

## 2.2 Synthesis of NSB Composite

1.0 g SDBS was dissolved in 50 mL deionized water to make SDBS solution. 1.0 g CS was dissolved in 50 mL 1% glacial acetic acid solution. These two solutions were mixed together. Adjust pH of the mixture to 9 with 1 mol L<sup>-1</sup> NaOH solution. Being stirred for 2 h, the mixture was put in an oven for drying at 50°C. Then the obtained solid product was calcined at 450°C for 2 h with the heating rate of 5°C min<sup>-1</sup> under a nitrogen atmosphere. The biochar was obtained after washing with dilute hydrochloric acid and deionized water and being dried at 50°C. The synthetic route was illustrated in Fig. 1.

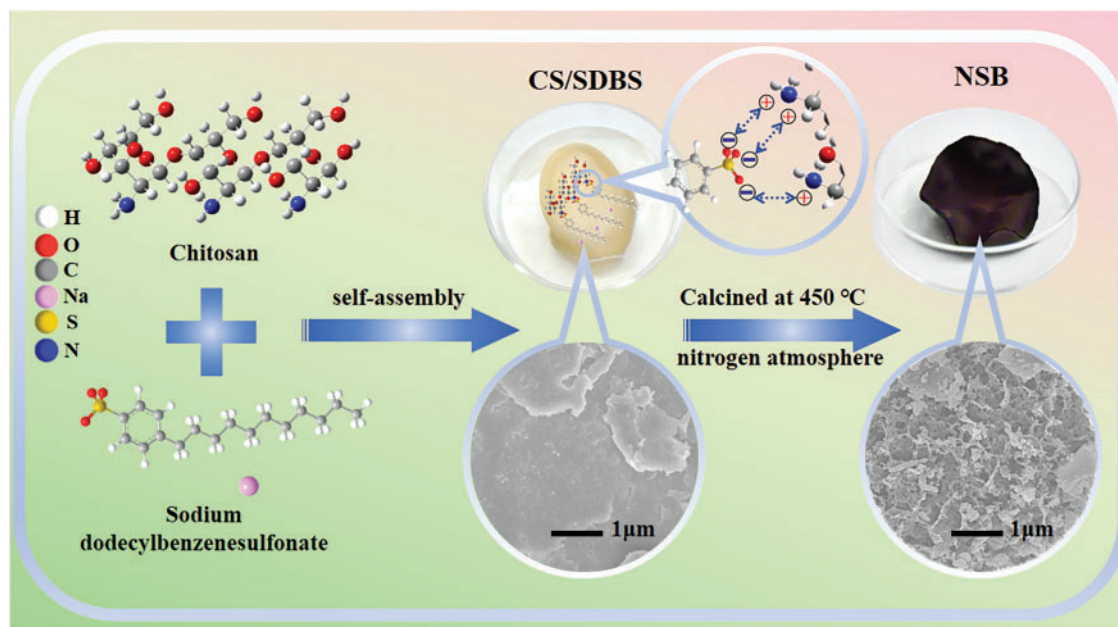


**Figure 1:** Diagram of the preparation of NSB

The prepared biochar was assumed to contain both N and S elements and named NSB. Meanwhile, SDBS and CS mixture at pH 9, -12 and -14 were studied. The resulted sample were named NSB-9, -12 and -14, respectively. In addition, the biochar obtained by calcining CS was named N-doped biochar (NB).

## 2.3 Characterization

X-ray diffraction (XRD, Japan Scientific Instruments Co., Ltd., Amagasaki-shi, Japan, D/max RB type) was used to analyze the structure using Cu *K* $\alpha$  ( $\lambda = 1.5418 \text{ \AA}$ ), and scanning rate of 5° min<sup>-1</sup>. The morphology was tested with field-emission scanning electron microscopy (SEM, Japan Electronics Corporation, Akishima-shi, Japan, JSM-7500F type). A physical adsorption analyzer (BET, multi station fully automatic specific surface area and porosity analyzer, American McMurdick Instruments Co., Ltd., Norcross, GA, USA, ASAP2460) to analyze the specific surface area and porosity of biochar. Fourier transform infrared spectrometer (FT-IR, Tianjin Gangdong Technology Development Co., Ltd., Tianjin, China FTIR-650 type) was used to analyze the functional groups in range of 400–4000 cm<sup>-1</sup>. X-ray photoelectron spectroscopy (XPS, Thermo Fisher Scientific, Waltham, MA, USA, K-Alpha type) to analyze the elemental chemical environment of biochar.

## 2.4 Adsorption Experiment

Adsorption experiment was carried out on 100 mL 100 mg L<sup>-1</sup> CTC solution at pH 7. 100 mg sample was used unless otherwise noted. At regular intervals, the solution was sampled and tested using UV-visible spectrophotometry at 366 nm. The adsorption capacity was calculated according to Eq. (1). The adsorption isothermal experiment was conducted on CTC in the concentration range from 20 to 200 mg L<sup>-1</sup> at 25°C. All the experiments were repeated for 3 times and the mean value was adopted.

$$Q_{\max} = \frac{(C_0 - C) \times V}{M} \quad (1)$$

herein,  $C_0$  and  $C$  (mg L<sup>-1</sup>) are the initial CTC concentration and the concentration at time  $t$  in solution, respectively;  $V$  is the initial solution volume (L) and  $M$  is the adsorbent mass (g).

To analyze the adsorption mechanism, the pseudo-first/second-order, Boyd and Elovich models were used to fit adsorption kinetic curves.

The first-order and second-order models were expressed by Eqs. (2) and (3).

$$\ln(Q_e - Q_t) = \ln Q_e - k_1 t \quad (2)$$

$$\frac{t}{Q_t} = \frac{1}{k_2 Q_e^2} + \frac{t}{Q_e} \quad (3)$$

herein,  $k_1$  (min<sup>-1</sup>) is the first-order reaction rate constant,  $k_2$  (g mg<sup>-1</sup> min<sup>-1</sup>) is the second-order reaction rate constant,  $Q_e$  (mg g<sup>-1</sup>) is the adsorption capacity at adsorption equilibrium, and  $t$  (min) is the adsorption time.

Boyd kinetics model was described by Eqs. (4) and (5) as follows:

$$F = \frac{q_t}{q_e} \quad (4)$$

$$B_t = -0.4997 - (1 - F) \quad (5)$$

where  $F$  is the fraction of organic materials adsorbed at time  $t$ .

Elovich kinetics model was described by Eq. (6).

$$Q_t = \frac{1}{\alpha} \ln(1 + abt) \quad (6)$$

The  $a$  and  $b$  are the equation constants [46].

Meanwhile, models of Langmuir, Freundlich, Temkin (T), Redlich-Peterson isotherm and Weber-Morris were also adopted to study adsorption behaviors of CTC.

Eqs. (7) and (8) were described for Langmuir or Freundlich models.

$$\frac{C_e}{Q_e} = \frac{1}{k_L Q_m} + \frac{C_e}{Q_m} \quad (7)$$

$$\lg C_e = \lg k_F + \left(\frac{1}{n}\right) \lg C_e \quad (8)$$

herein,  $k_L$  (mg<sup>-1</sup>) is a constant related to the adsorption energy, and  $Q_m$  (mg g<sup>-1</sup>) is the saturated adsorption capacity;  $k_F$  is a constant related to adsorption capacity, and  $1/n$  is a heterogeneous parameter related to adsorption strength.

Temkin and Redlich-Peterson isotherm models and Weber-Morris (W-M) intraparticle diffusion model were described by Eqs. (9)–(11), respectively.

$$Q_e = B \ln(AC_e) \quad (9)$$

herein,  $B = RT/b$  and  $b$  (J mol<sup>-1</sup>) is the Temkin constant related to the heat of adsorption, and  $A$  (L mg<sup>-1</sup>) is the equilibrium binding constant [47].

Redlich-Peterson isotherm was described by the Eq. (10):

$$N = KC(1 + aC^n) \quad (10)$$

herein,  $N$  (mg g<sup>-1</sup>) is the adsorption capacity at adsorption equilibrium, and  $C$  (mg L<sup>-1</sup>) is the concentration at equilibrium. The  $a$  and  $K$  are the Redlich-Peterson constants [48].

Weber-Morris intraparticle diffusion model was described by Eq. (11):

$$q_t = Kt^{1/2} + C \quad (11)$$

herein,  $q_t$  represents the adsorption capacity at time  $t$ .  $C$  is a constant related to the thickness, and  $K$  is the intraparticle diffusion rate constant [49].

The adsorption thermodynamics studies were carried out on 100 mg L<sup>-1</sup> CTC at 15°C, 25°C and 35°C. The relevant parameters were determined by Eqs. (12) and (13):

$$\Delta G = -RT \ln K_d \quad (12)$$

$$\ln K_d = -\frac{\Delta H}{RT} + \frac{\Delta S}{T} \quad (13)$$

where  $\Delta G$  (kJ mol<sup>-1</sup>) is the Gibbs free energy change,  $T$  (K) is absolute temperature,  $R$  is the universal gas constant (8.314 J mol<sup>-1</sup> K<sup>-1</sup>),  $K_d$  is the dimensionless thermodynamic equilibrium constant,  $\Delta H$  is the enthalpy change (kJ mol<sup>-1</sup>), and  $\Delta S$  is the entropy change (J mol<sup>-1</sup> K<sup>-1</sup>).

### 3 Results and Discussion

#### 3.1 Characterization of Catalyst

Fig. 2a illustrates the XRD patterns of NSB. All the samples have a wide peak at  $2\theta$  angles between 20° and 30°, which is typical diffraction of carbon [50]. FT-IR spectra are shown in Fig. 2b. The absorption peak at 1600 cm<sup>-1</sup> is attributed to C=O stretching vibration, and the wide peak located at 1000–1500 cm<sup>-1</sup> derives from C-O, C-C and C-N vibrations. It indicates multiple functional groups in NSB.

The chemical environments of C, O, N and S in NSB-12 were analyzed by XPS. To the C 1s spectrum (Fig. 2c), three peaks located at 284.6, 285.6 and 288.8 eV were fitted, which are the binding energies of C-C, C-N and C=O, respectively [51]. Fig. 2d is the O 1s XPS. The fitted two peaks at 532.3 and 533.3 eV correspond to the binding energies of C-O and C=O functional groups [52,53]. The XPS spectrum of N 1s was recorded from 390 to 410 eV. After fitting, three peaks at 398.2, 400.1 and 401.5 eV were obtained. They are the binding energies of pyridinium (N-6), pyrrole nitrogen (N-5), and graphitic nitrogen in NSB-12 [53–55]. It indicates that nitrogen was successfully doped into NSB. Meanwhile, peaks at 164.0 and 168.9 eV are attributed to S 2p. It indicates the presence of non-oxidizing sulfur such as thiophene sulfur in NSB-12. Strong peaks at 168.9 eV give the evidence that oxidized sulfur states, as sulfoxide and sulfone, are existing [56]. The calculated contents of C, O, N and S in NSB-12 are 88.4%, 9.9%, 0.9% and 0.8% according to XPS, respectively. The XPS results not only suggest the successful doping of N and S elements but also

present the diverse functional groups in NSB. These heteroatoms-contained functional groups may work as active sites during the adsorption and enhance the adsorption performance.

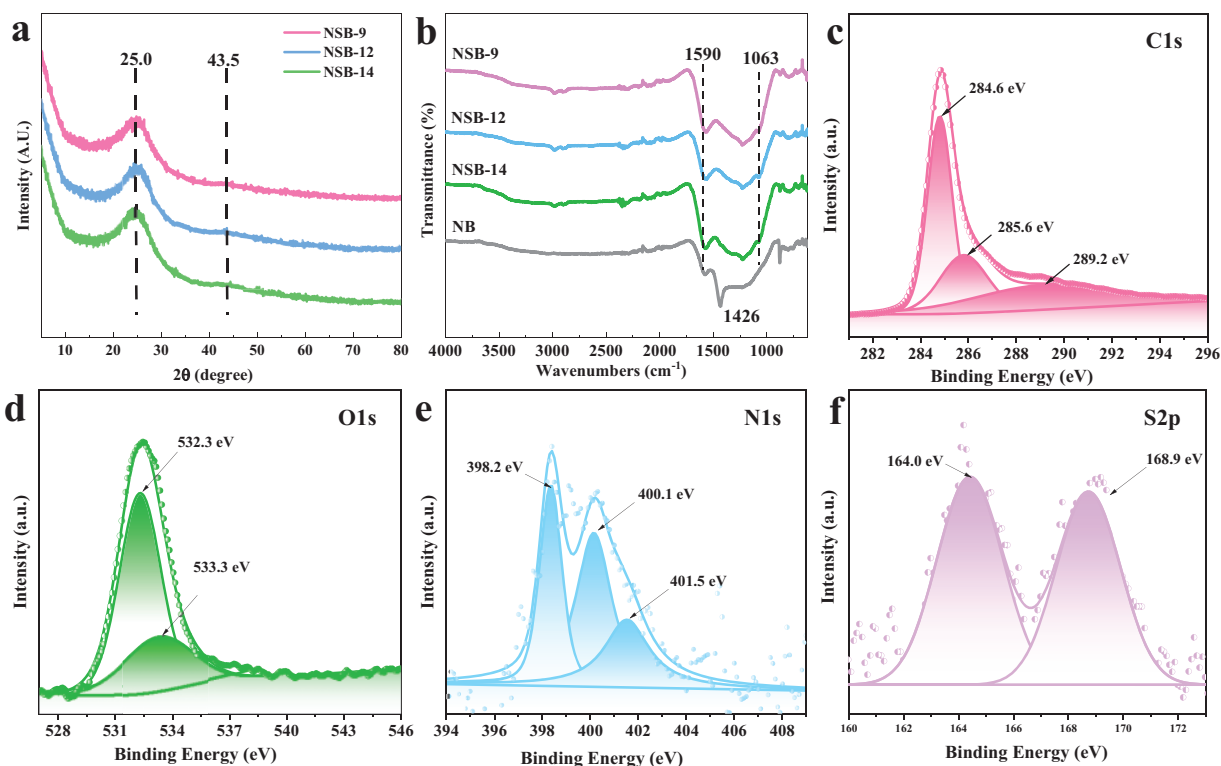


**Figure 2:** XRD patterns of (a) and FT-IR spectra (b) of NSBs, together with NSB-12 XPS spectra containing C 1s (c), O 1s (d), N 1s (e), and S 2p (f)

The micromorphology of NSBs was detected by SEM in Fig. 3. It can be seen that NB prepared without adding SDBS has fewer pores than NSB. Meanwhile, pores in NB are intact and isolated, showing no obvious interconnection with each other. To NSBs, hierarchical porous architectures could be observed. These pores are mutually connected and their walls are thinner than NB.

The difference in microstructures apparently results from the addition of SDBS. The self-assembling of CS and SDBS could occur. One can deduce that CS dissolves into water and its  $-NH_2$  groups are protonated in the acidic condition. Generally, CS carries positive charge. Differently, SDBS with  $-SO_3^-$  groups is negatively charged in the solution. The electrostatic attractions drive the self-assembling of SDBS and CS. The CS/SDBS complexes are formed. When increasing pH of the solution, CS deprotonates and CS/SDBS are deposited from the solution. Due to the long hydrophobic functional groups at the tail of SDBS, the CS aggregation could be hindered. Then NSB with the crossing linking porous architecture is obtained after calcination [57,58].

The higher pH is used during preparation, the more porous structure and the thinner of walls are produced in NSB. TEM of NSB-12 was also tested (Fig. 3e,f). It shows thin-layer and porous structure. The special morphology would endow NSB-12 with a high specific surface area. It even saves the activation operation. This would not only reduce preparation cost but also make the preparation process more environmentally friendly.

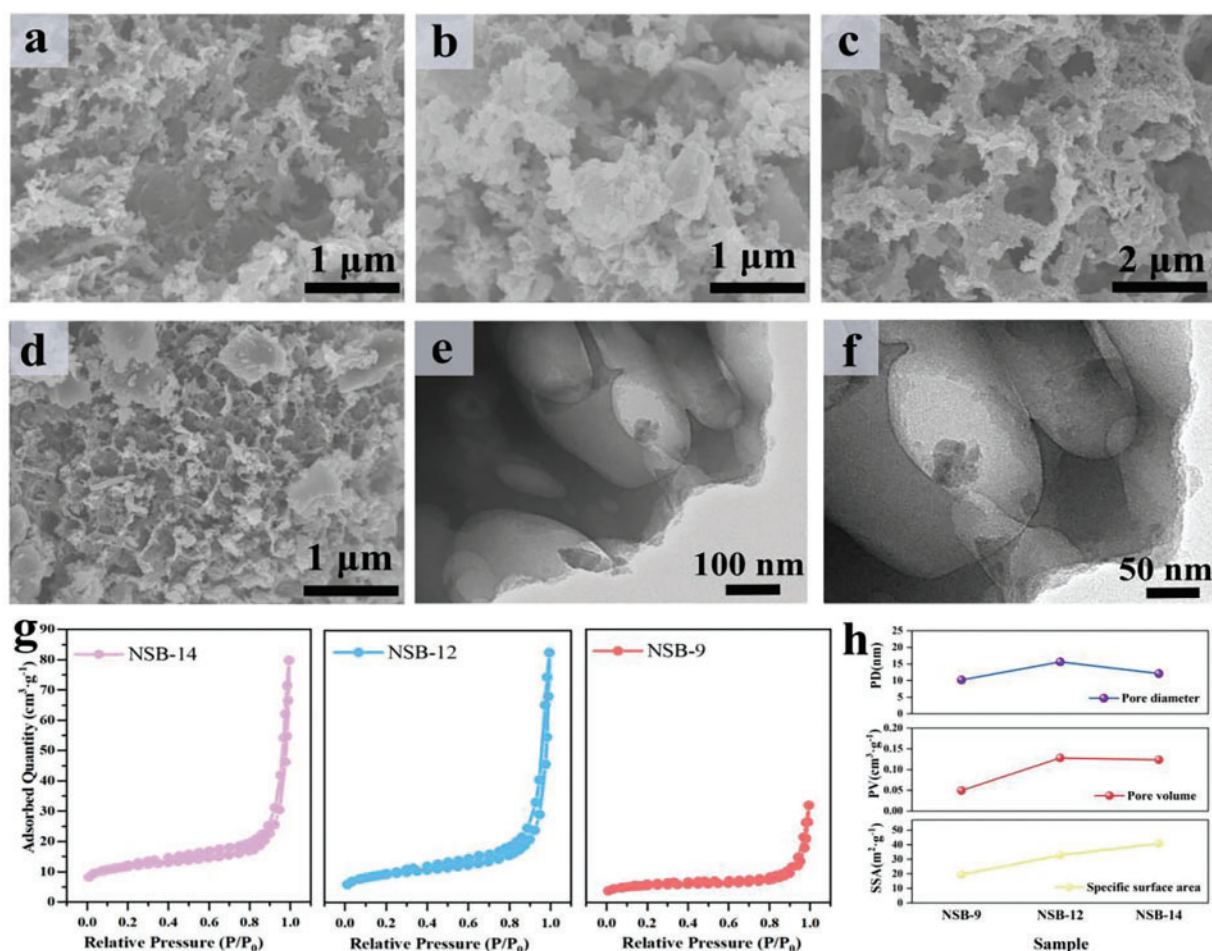


**Figure 3:** SEM images of NB (a), NSB-9 (b), NSB-12 (c) and NSB-14 (d), TEM images of NSB-12 (e, f), the nitrogen adsorption/desorption isotherms of NSBs (g), and pore diameter, pore volume and specific surface areas of NSBs (h)

The BET specific surface areas of NSBs were tested by  $N_2$  adsorption/desorption experiments. The adsorption isotherms are shown in Fig. 3g,h. The specific surface area increases with the increasement of pH during preparation. NSB-14 is the highest ( $40.8 \text{ m}^2 \text{ g}^{-1}$ ), along with NSB-12 ( $32.8 \text{ m}^2 \text{ g}^{-1}$ ) and NSB-9 ( $19.4 \text{ m}^2 \text{ g}^{-1}$ ). Though the specific surface area is quite low compared to those carbon prepared by the activation, the pore volume of NSB-14 is large. It reaches  $0.12 \text{ cm}^3 \text{ g}^{-1}$ , which may indicate that pores formed in this way are meso/macro ones.

### 3.2 Absorption Performance

Absorption performance of NSBs was fully evaluated by CTC. Fig. 4a is the adsorption capacities of samples after 4 h operation. One can see that NSBs show equilibrium adsorption capacity  $q_e$  in the range of  $60\sim 70 \text{ mg g}^{-1}$ . They all are much larger than NB ( $38.6 \text{ mg g}^{-1}$ ). The  $q_e$  value of NSB-12 can reach  $59.3 \text{ mg g}^{-1}$ , which is 155% higher than NB. One can notice that NSB-14 has even higher  $q_e$  of  $66.1 \text{ mg g}^{-1}$ . However, during the preparation of NSB-14, a large amount alkali was required to raise pH from 12 to 14. Thus, NSB-12 was considered as the most cost-effective sample among all NSBs.

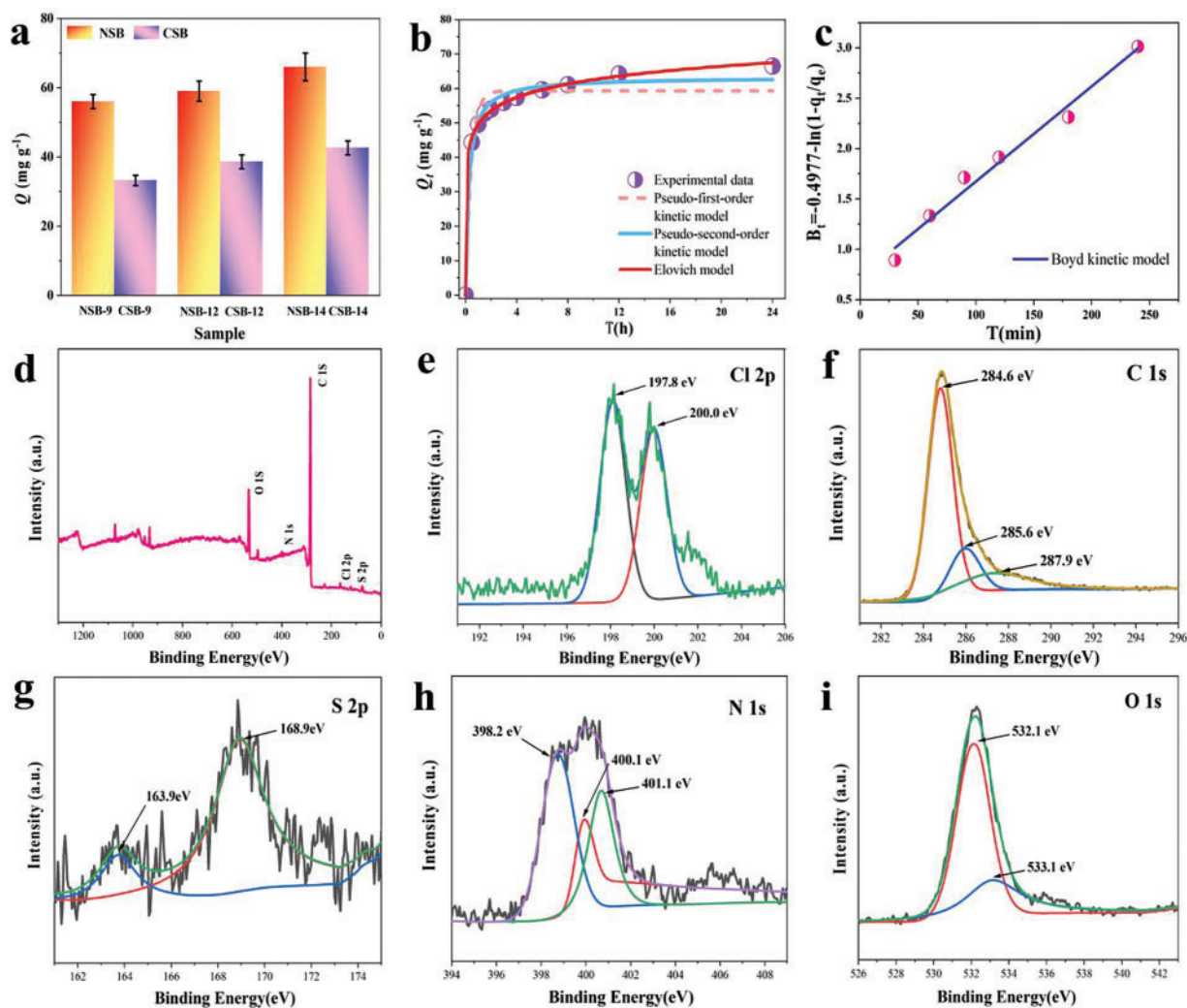


**Figure 4:** Adsorption capacities (a), adsorption kinetic curve of NSB-12 and its fitting plots (b), Boyd kinetic model fitting plot (c), XPS spectrum of NSB-12 after loaded with CTC, survey spectrum (d), Cl 2p (e), C 1s (f), S 2p (g), N 1s (h) and O 1s (i)

The kinetics of NSB-12 in Fig. 4b show that the adsorption rate to CTC is fast. It can achieve 44.4 mg g<sup>-1</sup> capacity in 30 min and get to the equilibrium by taking 4 h. Both quasi-first/second-order kinetic models of Elovich and Boyd were used to fit the adsorption process (Fig. 4b,c and Table 1).  $R^2$  of 0.9868 was obtained for the quasi-second-order model, being higher than that of the quasi-first-order model (0.9503). Additionally,  $q_e$  calculated by the quasi-second-order kinetic model is 63.3 mg g<sup>-1</sup>, which is close to experimental data. This means adsorption process is more accurately described by the quasi-second-order kinetic model. A chemical adsorption is involved. The correlation coefficients  $R^2$  of 0.9990 and 0.9820 were obtained by Elovich and Boyd fittings. It indicates the heterogeneous surface of NSB and multiple mechanism including intraparticle diffusion are involved in the adsorption process [59].

It is deduced that the heteroatoms-related functional groups play an important role during adsorption. To further prove it, XPS after adsorption was performed. And results were shown in Fig. 4d-i. In the survey spectrum, peaks of binding energies of C 1s, S 2p, N 1s, O 1s and Cl 2p are found. Meanwhile, the spectrum of Cl 2p exhibits doublet peak at binding energies of 197.9 and 200 eV. These results give the evidence that

CTC has been successfully adsorbed onto NSB. The C 1s spectrum remains similar before and after adsorbing CTC by NSB (Figs. 2c and 4f). Spectra of N 1s and S 2p of NSB show close binding energies before and after adsorption. However, the integral areas of peaks at 400.1 eV (N 1s) and 163.9 eV (S 2p) decrease greatly. These results indicate that the doped N and S may participate in the adsorption process, which cause the heterogeneous surface [60,61]. Meanwhile, the two peaks observed in the O 1s spectrum correspond to C-O/C=O (532.1 eV) and -OH (533.1 eV), respectively. After CTC adsorption, the binding energies of O1s shift by 0.2 eV compared to ones of NSB. It is because of hydrogen bonds between NSB and CTC [62].

**Table 1:** Kinetic model fitting parameters of NSB-12

Sample	Pseudo-first-order			Pseudo-second-order		
	$q_e$ (mg g <sup>-1</sup> )	$k_1$ (min <sup>-1</sup> )	R <sup>2</sup>	$q_e$ (mg g <sup>-1</sup> )	$k_2$ (g mg <sup>-1</sup> min <sup>-1</sup> )	R <sup>2</sup>
NSB-12	59.3	2.2504	0.9503	63.3	0.0604	0.9868

Effects of different CTC initial concentrations were also studied. The concentration ranges from 20 to 200 mg L<sup>-1</sup>. The adsorption isotherm curves of NSB-12 are presented in Fig. 5a. It can be seen that the higher the concentration is, the larger adsorption capacity is. The maximum adsorption capacity ( $q_{max}$ ) reaches 101.3 mg g<sup>-1</sup> after 24 h adsorption. Langmuir, Freundlich and Redlich-Peterson models were used to fit the isotherms obtained at 12 h (Fig. 4d and Table 2). The correlation coefficient R<sup>2</sup> is 0.9737 for Langmuir model, revealing the adsorption process for CTC can be better described by the Langmuir model. It suggests that the adsorption is primarily of single-molecular layer adsorption. The correlation coefficient R<sup>2</sup> obtained from Redlich-Peterson model is 0.9910. It indicates a complicated adsorption mechanism. Non-ideal monolayer adsorption and nonuniform multilayer adsorption on the surface may coexist [63].

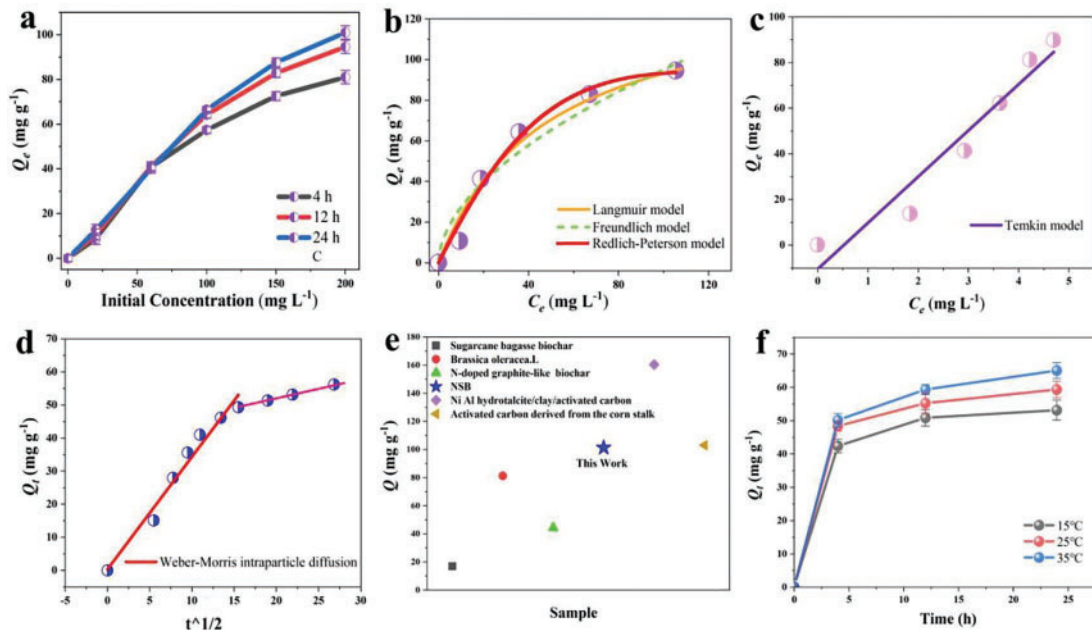


**Figure 5:** Adsorption isotherms of NSB-12 with different time (a) and fitting plots obtained by Langmuir, Freundlich and Redlich-Peterson models (b), Temkin model (c), Weber-Morris intraparticle diffusion model (d), adsorption performance with different materials (e) and adsorption kinetics at different temperatures (f)

**Table 2:** Fitting parameters of NSB-12 by Langmuir and Freundlich models

Adsorption time	Langmuir			Freundlich		
	$q_{\max}$ (mg g <sup>-1</sup> )	$k_L$ (L mg <sup>-1</sup> )	R <sup>2</sup>	$n$	$k_F$	R <sup>2</sup>
12 h	137.7	0.0209	0.9737	1.8439	7.8268	0.9393

Meanwhile, both Temkin and Weber-Morris intraparticle diffusion models were applied to fit adsorption isotherms in Fig. 5c,d. The correlation coefficient R<sup>2</sup> from Temkin is 0.9348. Intermolecular interactions, such as electrostatic attraction or hydrogen bond between NSB and CTC, play an important role during the adsorption. Fitting plots with Weber-Morris model find that the adsorption process consists of two stages. In the first one, the intercept of the straight line is small, indicating the fast adsorption rate is controlled by external surface uptake; and the second stage shows a relatively slow rate, which is mainly dominated by intraparticle diffusion. The results further prove that the adsorption may be controlled by multiple mechanism [64].

The adsorption performance of NSB-12 and relevant materials was summarized in Fig. 5e [65–69]. Compared to other biochar materials, NSB-12 exhibits the superior adsorption activity towards CTC. Exemplarily, its adsorption capacity to CTC is doubled that of N-doped graphite-like mesoporous structure biochar prepared by furfural residue (44.3 mg g) [68].

The observed adsorption behavior can be attributed to the presence of diverse functional groups in NSBs, including -SO<sub>3</sub>H, -NH<sub>2</sub>, C=O, -OH, and pyridine nitrogen groups. These functional groups facilitate electron transfer and bond formation with CTC and then enhance adsorption efficiency. Furthermore, fittings by Freundlich model reveal that heterogeneous multilayer adsorption also occurs between NSB and CTC. This suggests that hydrogen bonding and electrostatic interactions between zwitterionic species within CTC and NSB also significantly influence the overall adsorption process [70].

To investigate the temperature effect, adsorption experiments on 100 mg L<sup>-1</sup> CTC solution at 15°C, 25°C, and 35°C were carried out. The results are shown in Fig. 5f and Table 3. As the adsorption temperature raises from 15°C to 35°C, the uptake of CTC increases from 53.1 to 65.2 mg g<sup>-1</sup>. Negative ΔG, and positive ΔS and ΔH indicate that CTC is spontaneously adsorbed onto NSB-12 surface; and the adsorption is an endothermic process [71]. The more negative value of ΔG while raising temperature indicates that high temperature can improve the adsorption performance [72].

**Table 3:** Thermodynamics parameters for adsorption of CTC by NSB-12

T (k)	ΔG (kJ mol <sup>-1</sup> )	ΔH (kJ mol <sup>-1</sup> )	ΔS (J mol <sup>-1</sup> K <sup>-1</sup> )
288	-0.297	18.71	65.95
298	-0.932		
308	-1.585		

### 3.3 Effect of pH, Ionic Strength and Stability on Adsorption

Effect of pH was studied as shown in Fig. 6a. The largest adsorption capacity was obtained when the solution pH is 7. To understand this, the pH of zero point charge (pH<sub>ZPC</sub>) of NSB-12 was determined by pH drift method [73]. It gives pH<sub>ZPC</sub> of 6 in Fig. 6b. This means the surface of NSB-12 is positively charged while solution pH below 6, and negatively charged above 6. Meanwhile, the ionization equilibrium constants

of CTC solution are 3.3 ( $pK1$ ) and 7.44 ( $pK2$ ) [74]. Therefore, CTC could carry positive charge when pH is under 8; and it would carry negative charge when pH is 8 or higher. That means both NSB and CTC have the same sorts of charges under acid/basic conditions, which would be electrostatically repulsive and reduce adsorption capacity [75]. When the pH value of solution is 7, CTC is positively charged and NSB is negatively charged. The electrostatic attraction between them would enhance the adsorption performance [76]. Thus, NSB shows the best adsorption performance to CTC at the neutral condition.

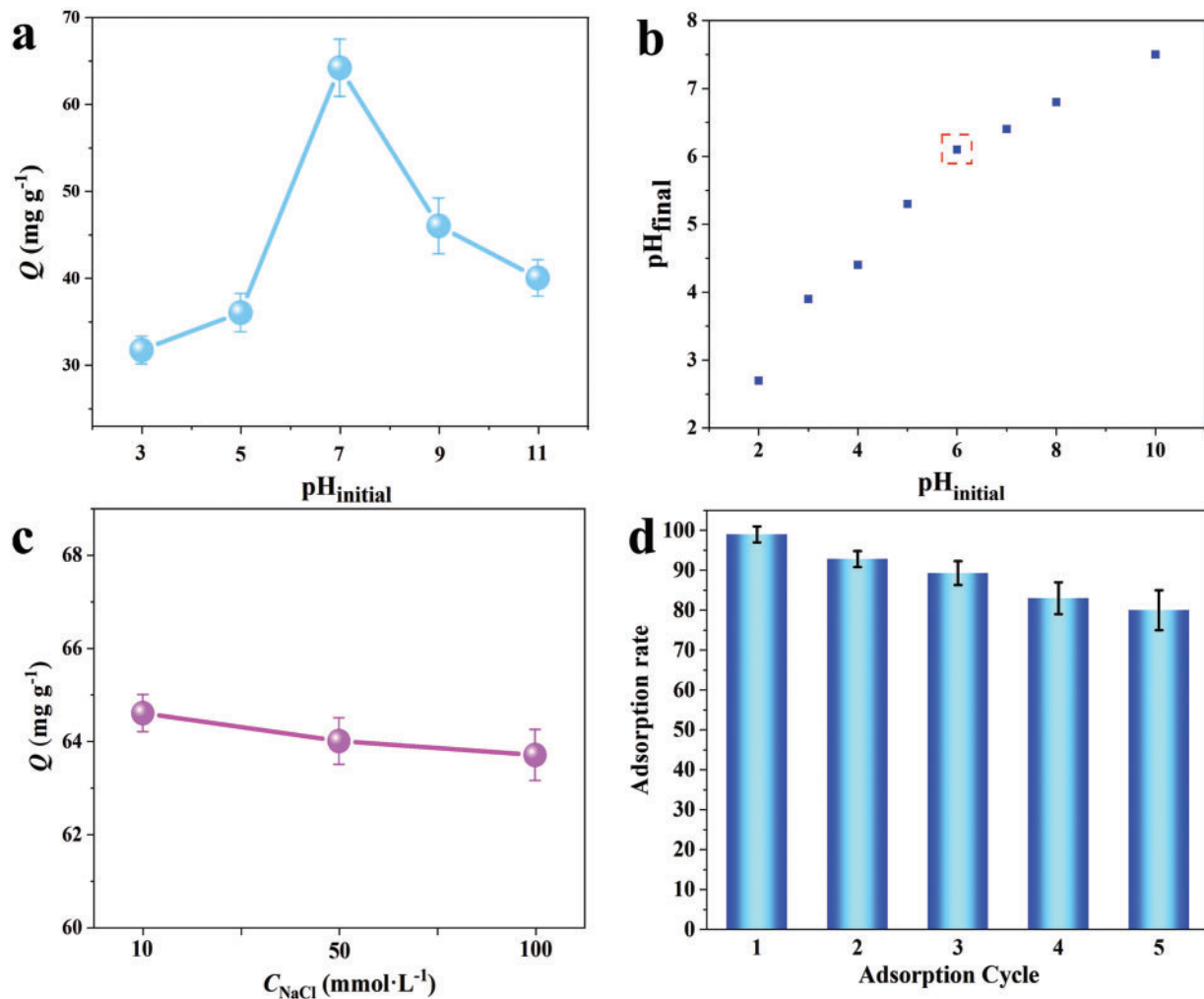


**Figure 6:** Adsorption of NSB-12 to CTC solution with different pH values (a) and pH variation in terms of initial pH of solution for determination of point of zero charge pH (b) and NaCl concentrations (c) for 12 h and adsorption in different adsorption cycles (d)

Fig. 6c illustrates the adsorption experiments in different NaCl concentrations. One can see that with the increase of salt concentration, the adsorption capacity of NSB remains stable. Generally, high ionic strength in the solution could weaken the electrostatic interaction between ionic compounds and surface functional groups of adsorbent materials through shielding effect, thereby diminishing the adsorption performance. However, during the adsorption of CTC by NSB, the influence of non-covalent interaction, such as electrostatic force, is relatively minor. This is in good agreement with the adsorption process we mentioned previously. It is mainly of chemical adsorption, thus barely affecting the adsorption performance.

To study the stability of NSB, the cyclic adsorption was carried out. To 100 mL 100 mg L<sup>-1</sup> CTC solution, 100 mg NSB-12 was added. And then shake it at 25°C for 4 h. After that, the obtained NSB-CTC was filtered and put into 100 mL solution for desorption at 25°C for 12 h. The solution was made by 1 mol L<sup>-1</sup> H<sub>2</sub>O<sub>2</sub> and 0.01 mol L<sup>-1</sup> ammonium persulfate. After five cyclic experiments, the adsorption capacity of NSB-12 still keeps 80% as shown in Fig. 6d.

#### 4 Conclusions

In this work, SDBS was used as structure guidance in complexing with CS. SDBS also served as sulfur source and CS provided nitrogen source to successfully prepare N, S dually-doped biochar (NSB). Modulating the interaction of CS and SDBS helped fabricate thin-layer and porous structures. Our synthetic approach was developed by saving the activation operation and the second step calcination. Due to numerous pores, doped heteroatoms and abundant functional groups, NSB shows good adsorption properties towards CTC. Its adsorption capacity gets to 101.3 mg g<sup>-1</sup> with a fast rate and good recycling stability. The capacity is twice higher than that of NB prepared by only CS. Analyses of adsorption kinetics and isotherms realize that the adsorption process is controlled by multiple mechanisms. It includes the electrostatic attraction and intermolecular force. Certainly, there is still room to improve the adsorption capacity of our material, and more types of antibiotics will be attempted for further application. In brief, the current NSB material could be blooming for CTC antibiotic treatment due to its merits of renewable and low-cost raw materials and a simplified synthesis strategy.

**Acknowledgement:** Not applicable.

**Funding Statement:** This work is supported by the National Natural Science Foundation of China (22276046).

**Author Contributions:** Jun-Jie Yang: Writing—original draft, Investigation, Formal analysis; Ran An: Data curation, Investigation; Jing-Heng Nie: Data curation, Investigation; Hao-Miao Ma: Investigation, Formal analysis; Yu-Qing Yan: Investigation, Formal analysis; Yuan-Ru Guo: Writing—review & editing, Supervision, Conceptualization; Qing-Jiang Pan: Writing—review & editing. All authors reviewed the results and approved the final version of the manuscript.

**Availability of Data and Materials:** Data will be made available on request.

**Ethics Approval:** Not applicable.

**Conflicts of Interest:** The authors declare no conflicts of interest to report regarding the present study.

#### References

1. Ahmad F, Zhu D, Sun J. Environmental fate of tetracycline antibiotics: degradation pathway mechanisms, challenges, and perspectives. *Environ Sci Eur.* 2021;33(1):64. doi:10.1186/s12302-021-00505-y.
2. Leichtweis J, Vieira Y, Welter N, Silvestri S, Dotto GL, Carissimi E. A review of the occurrence, disposal, determination, toxicity and remediation technologies of the tetracycline antibiotic. *Process Saf Environ Prot.* 2022;160:25–40. doi:10.1016/j.psep.2022.01.085.
3. Yang W, Li J, Yao Z, Li M. A review on the alternatives to antibiotics and the treatment of antibiotic pollution: current development and future prospects. *Sci Total Environ.* 2024;926(8):171757. doi:10.1016/j.scitotenv.2024.171757.
4. Sum PE, Sum FW, Projan SJ. Recent developments in tetracycline antibiotics. *Curr Pharm Des.* 1998;4(2):119–32. doi:10.2174/138161280401221007113202.
5. Wallace JS, Garner E, Pruden A, Aga DS. Occurrence and transformation of veterinary antibiotics and antibiotic resistance genes in dairy manure treated by advanced anaerobic digestion and conventional treatment methods. *Environ Pollut.* 2018;236(Suppl. 1):764–72. doi:10.1016/j.envpol.2018.02.024.

6. Ji Y, Shi Y, Dong W, Wen X, Jiang M, Lu J. Thermo-activated persulfate oxidation system for tetracycline antibiotics degradation in aqueous solution. *Chem Eng J.* 2016;298(3):225–33. doi:10.1016/j.cej.2016.04.028.
7. Pimentel JAI, Dong CD, Garcia-Segura S, Abarca RRM, Chen CW, de Luna MDG. Degradation of tetracycline antibiotics by Fe<sup>2+</sup>-catalyzed percarbonate oxidation. *Sci Total Environ.* 2021;781:146411. doi:10.1016/j.scitotenv.2021.146411.
8. Shi Y, Lin H, Ma J, Zhu R, Sun W, Lin X, et al. Degradation of tetracycline antibiotics by *Arthrobacter nicotianae* OTC-16. *J Hazard Mater.* 2021;403:123996. doi:10.1016/j.jhazmat.2020.123996.
9. Wang H, Chen T, Chen D, Zou X, Li M, Huang F, et al. Sulfurized oolitic hematite as a heterogeneous Fenton-like catalyst for tetracycline antibiotic degradation. *Appl Catal B Environ.* 2020;260(2):118203. doi:10.1016/j.apcatb.2019.118203.
10. Wei J, Liu Y, Zhu Y, Li J. Enhanced catalytic degradation of tetracycline antibiotic by persulfate activated with modified sludge bio-hydrochar. *Chemosphere.* 2020;247:125854. doi:10.1016/j.chemosphere.2020.125854.
11. Zhao N, Liu K, Yan B, Zhu L, Zhao C, Gao J, et al. Chlorotetracycline hydrochloride removal by different biochar/Fe composites: a comparative study. *J Hazard Mater.* 2021;403:123889. doi:10.1016/j.jhazmat.2020.123889.
12. Du L, Ahmad S, Liu L, Wang L, Tang J. A review of antibiotics and antibiotic resistance genes (ARGs) adsorption by biochar and modified biochar in water. *Sci Total Environ.* 2023;858(Pt 2):159815. doi:10.1016/j.scitotenv.2022.159815.
13. Qiao D, Qu X, Chen X, Sun B, Ding W, Chen C, et al. Rational structural design of graphene oxide/W<sub>18</sub>O<sub>49</sub> nanocomposites realizes highly efficient removal of tetracycline in water. *Appl Surf Sci.* 2023;619(15):156630. doi:10.1016/j.apsusc.2023.156630.
14. Valizadeh K, Bateni A, Sojoodi N, Rafiei R, Behrozi AH, Maleki A. Preparation and characterization of chitosan-curdlan composite magnetized by zinc ferrite for efficient adsorption of tetracycline antibiotics in water. *Int J Biol Macromol.* 2023;235(5):123826. doi:10.1016/j.ijbiomac.2023.123826.
15. Yakout AA, Alshitari W, Akhdhar A. Synergistic effect of Cu-nanoparticles and β-cyclodextrin functionalized reduced graphene oxide nanocomposite on the adsorptive remediation of tetracycline antibiotics. *Carbohydr Polym.* 2021;273(6):118528. doi:10.1016/j.carbpol.2021.118528.
16. Zou SJ, Chen YF, Zhang Y, Wang XF, You N, Fan HT. A hybrid sorbent of α-iron oxide/reduced graphene oxide: studies for adsorptive removal of tetracycline antibiotics. *J Alloys Compd.* 2021;863:158475. doi:10.1016/j.jallcom.2020.158475.
17. Choi KJ, Kim SG, Kim SH. Removal of antibiotics by coagulation and granular activated carbon filtration. *J Hazard Mater.* 2008;151(1):38–43. doi:10.1016/j.jhazmat.2007.05.059.
18. Khaledi K, Valdes Labrada GM, Soltan J, Predicala B, Nemati M. Adsorptive removal of tetracycline and lincomycin from contaminated water using magnetized activated carbon. *J Environ Chem Eng.* 2021;9(5):105998. doi:10.1016/j.jece.2021.105998.
19. Nie Y, Zhao C, Zhou Z, Kong Y, Ma J. Hydrochloric acid-modified fungi-microalgae biochar for adsorption of tetracycline hydrochloride: performance and mechanism. *Bioresour Technol.* 2023;383(11):129224. doi:10.1016/j.biortech.2023.129224.
20. Gurunathan S, Kim JH. Synthesis, toxicity, biocompatibility, and biomedical applications of graphene and graphene-related materials. *Int J Nanomedicine.* 2016;11:1927–45. doi:10.2147/IJN.
21. Malhotra R, Halbig CE, Sim YF, Lim CT, Leong DT, Castro Neto AH, et al. Cytotoxicity survey of commercial graphene materials from worldwide. *npj 2D Mater Appl.* 2022;6(1):65. doi:10.1038/s41699-022-00330-8.
22. Novais RM, Caetano APF, Seabra MP, Labrincha JA, Pullar RC. Extremely fast and efficient methylene blue adsorption using eco-friendly cork and paper waste-based activated carbon adsorbents. *J Clean Prod.* 2018;197:1137–47. doi:10.1016/j.jclepro.2018.06.278.
23. Ullah S, Ahmad Shah SS, Altaf M, Hossain I, El Sayed ME, Kallel M, et al. Activated carbon derived from biomass for wastewater treatment: synthesis, application and future challenges. *J Anal Appl Pyrolysis.* 2024;179(3):106480. doi:10.1016/j.jaap.2024.106480.
24. Ge L, Zhao C, Zuo M, Tang J, Ye W, Wang X, et al. Review on the preparation of high value-added carbon materials from biomass. *J Anal Appl Pyrolysis.* 2022;168(5):105747. doi:10.1016/j.jaap.2022.105747.

25. Swami S, Sahu SN, Shrivastava R. Nanomaterial catalyzed green synthesis of tetrazoles and its derivatives: a review on recent advancements. *RSC Adv.* 2021;11(62):39058–86. doi:10.1039/D1RA05955F.
26. Xia D, Yu H, Li H, Huang P, Li Q, Wang Y. Carbon-based and carbon-supported nanomaterials for the catalytic conversion of biomass: a review. *Environ Chem Lett.* 2022;20(3):1719–44. doi:10.1007/s10311-022-01402-3.
27. Mohanty AK, Vivekanandhan S, Das O, Romero Millán LM, Klinghoffer NB, Nzihou A, et al. Biocarbon materials. *Nat Rev Meth Primers.* 2024;4(1):19. doi:10.1038/s43586-024-00297-4.
28. Yu S, He J, Zhang Z, Sun Z, Xie M, Xu Y, et al. Towards negative emissions: hydrothermal carbonization of biomass for sustainable carbon materials. *Adv Mater.* 2024;36(18):e2307412. doi:10.1002/adma.202307412.
29. Jiao H, Guo X, Shu F, Zhang Q, Wu W, Jin Y, et al. Structure-property-function relationships of wood-based activated carbon in energy and environment materials. *Sep Purif Technol.* 2025;353:128607. doi:10.1016/j.seppur.2024.128607.
30. Ndagijimana P, Rong H, Ndokoye P, Mwizerwa JP, Nkinahamira F, Luo S, et al. A review on activated carbon/graphene composite-based materials: synthesis and applications. *J Clean Prod.* 2023;417(1):138006. doi:10.1016/j.jclepro.2023.138006.
31. Lin Z, Wang R, Tan S, Zhang K, Yin Q, Zhao Z, et al. Nitrogen-doped hydrochar prepared by biomass and nitrogen-containing wastewater for dye adsorption: effect of nitrogen source in wastewater on the adsorption performance of hydrochar. *J Environ Manage.* 2023;334:117503. doi:10.1016/j.jenvman.2023.117503.
32. Wang B, Lan J, Bo C, Gong B, Ou J. Adsorption of heavy metal onto biomass-derived activated carbon: review. *RSC Adv.* 2023;13(7):4275–302. doi:10.1039/D2RA07911A.
33. Zhi F, Zhou W, Chen J, Meng Y, Hou X, Qu J, et al. Adsorption properties of active biochar: overlooked role of the structure of biomass. *Bioresour Technol.* 2023;387(3):129695. doi:10.1016/j.biortech.2023.129695.
34. Chen J, Zhou J, Zheng W, Leng S, Ai Z, Zhang W, et al. A complete review on the oxygen-containing functional groups of biochar: formation mechanisms, detection methods, engineering, and applications. *Sci Total Environ.* 2024;946:174081. doi:10.1016/j.scitotenv.2024.174081.
35. Gao L, Li Z, Yi W, Wang L, Zhang P, Wan Z, et al. Quantitative contribution of minerals and organics in biochar to Pb(II) adsorption: considering the increase of oxygen-containing functional groups. *J Clean Prod.* 2021;325:129328. doi:10.1016/j.jclepro.2021.129328.
36. Wu S, Fang G, Wang Y, Zheng Y, Wang C, Zhao F, et al. Redox-active oxygen-containing functional groups in activated carbon facilitate microbial reduction of ferrihydrite. *Environ Sci Technol.* 2017;51(17):9709–17. doi:10.1021/acs.est.7b01854.
37. Kern M, Škulj S, Rožman M. Adsorption of a wide variety of antibiotics on graphene-based nanomaterials: a modelling study. *Chemosphere.* 2022;296:134010. doi:10.1016/j.chemosphere.2022.134010.
38. Zandipak R, Sobhanardakani S. Novel mesoporous Fe<sub>3</sub>O<sub>4</sub>/SiO<sub>2</sub>/CTAB-SiO<sub>2</sub> as an effective adsorbent for the removal of amoxicillin and tetracycline from water. *Clean Technol Environ Policy.* 2018;20(4):871–85. doi:10.1007/s10098-018-1507-5.
39. Hammi N, Chen S, Dumeignil F, Royer S, El Kadib A. Chitosan as a sustainable precursor for nitrogen-containing carbon nanomaterials: synthesis and uses. *Mater Today Sustain.* 2020;10:100053. doi:10.1016/j.mtsust.2020.100053.
40. Khan A, Goepel M, Colmenares JC, Gläser R. Chitosan-based N-doped carbon materials for electrocatalytic and photocatalytic applications. *ACS Sustain Chem Eng.* 2020;8(12):4708–27. doi:10.1021/acssuschemeng.9b07522.
41. Wang S, Zhang X, Tang Y, Hao S, Zheng S, Qiao J, et al. Facile fabrication of biomass chitosan-derived magnetic carbon aerogels as multifunctional and high-efficiency electromagnetic wave absorption materials. *Carbon.* 2024;216(25):118528. doi:10.1016/j.carbon.2023.118528.
42. Santos VP, Marques NSS, Maia PCSV, Lima MAB, Franco LO, Campos-Takaki GM. Seafood waste as attractive source of chitin and chitosan production and their applications. *Int J Mol Sci.* 2020;21(12):E4290. doi:10.3390/ijms21124290.
43. Chen G, Wang H, Han L, Yang N, Hu B, Qiu M, et al. Highly efficient removal of U(VI) by a novel biochar supported with FeS nanoparticles and chitosan composites. *J Mol Liq.* 2021;327:114807. doi:10.1016/j.molliq.2020.114807.

44. Li J, Liu M, Niu G, Xiong Q, Ma Y, An R, et al. Enhanced anti-corrosion performances of epoxy resin using the addition of sodium dodecylbenzene sulfonate-modified graphene. *Coatings*. 2021;11(6):655. doi:10.3390/coatings11060655.
45. Zhao L, Zhang Q, Li X, Ye J, Chen J. Adsorption of Cu(II) by phosphogypsum modified with sodium dodecyl benzene sulfonate. *J Hazard Mater*. 2020;387:121808. doi:10.1016/j.jhazmat.2019.121808.
46. Sobhanardakani S, Zandipak R. 2, 4-Dinitrophenylhydrazine functionalized sodium dodecyl sulfate-coated magnetite nanoparticles for effective removal of Cd(II) and Ni(II) ions from water samples. *Environ Monit Assess*. 2015;187(7):412. doi:10.1007/s10661-015-4635-y.
47. Valizadeh R, Mahdavian L. Phytoremediation and adsorption isotherms of heavy metal ions by *Convolvulus tricolor* (CTC). *Int J Phytoremediat*. 2016;18(4):329–36. doi:10.1080/15226514.2015.1094449.
48. Sobhanardakani S, Zandipak R. Synthesis and application of TiO<sub>2</sub>/SiO<sub>2</sub>/Fe<sub>3</sub>O<sub>4</sub> nanoparticles as novel adsorbent for removal of Cd(II), Hg(II) and Ni(II) ions from water samples. *Clean Technol Environ Policy*. 2017;19(7):1913–25. doi:10.1007/s10098-017-1374-5.
49. Zhang H, Tian S, Zhu Y, Zhong W, Qiu R, Han L. Insight into the adsorption isotherms and kinetics of Pb (II) on pellet biochar via *in situ* non-destructive 3D visualization using micro-computed tomography. *Bioresour Technol*. 2022;358(1):127406. doi:10.1016/j.biortech.2022.127406.
50. Huo S, Liu M, Wu L, Liu M, Xu M, Ni W, et al. Methanesulfonic acid-assisted synthesis of N/S co-doped hierarchically porous carbon for high performance supercapacitors. *J Power Sources*. 2018;387:81–90. doi:10.1016/j.jpowsour.2018.03.061.
51. Peng L, Peng H, Hung CT, Guo D, Duan L, Ma B, et al. Programmable synthesis of radially gradient-structured mesoporous carbon nanospheres with tunable core-shell architectures. *Chem*. 2021;7(4):1020–32. doi:10.1016/j.chempr.2021.01.001.
52. Cheng BH, Deng LJ, Jiang J, Jiang H. Catalytic cycloaddition of CO<sub>2</sub> to epoxides by the synergistic effect of acidity and alkalinity in a functionalized biochar. *Chem Eng J*. 2022;442:136265. doi:10.1016/j.cej.2022.136265.
53. Sun Y, Xu D, Wang S. Self-assembly of biomass derivatives into multiple heteroatom-doped 3D-interconnected porous carbon for advanced supercapacitors. *Carbon*. 2022;199(33):258–67. doi:10.1016/j.carbon.2022.08.026.
54. Huang K, Yang S, Liu X, Zhu C, Qi F, Wang K, et al. Adsorption of antibiotics from wastewater by cabbage-based N,P Co-doped mesoporous carbon materials. *J Clean Prod*. 2023;391(3):136174. doi:10.1016/j.jclepro.2023.136174.
55. Shi J, Yan N, Cui H, Xu J, Liu Y, Zhang S. Salt template synthesis of nitrogen and sulfur co-doped porous carbons as CO<sub>2</sub> adsorbents. *ACS Sustainable Chem Eng*. 2019;7(24):19513–21. doi:10.1021/acssuschemeng.9b04574.
56. Shi J, Yan N, Cui H, Liu Y, Weng Y. Sulfur doped microporous carbons for CO<sub>2</sub> adsorption. *J Environ Chem Eng*. 2017;5(5):4605–11. doi:10.1016/j.jece.2017.09.002.
57. Goddard ED. Polymer/surfactant interaction: interfacial aspects. *J Colloid Interface Sci*. 2002;256(1):228–35. doi:10.1006/jcis.2001.8066.
58. Márton P, Áder L, Kemény DM, Rácz A, Kovács D, Nagy N, et al. Chitosan-surfactant composite nanocoatings on glass and zinc surfaces prepared from aqueous solutions. *Molecules*. 2024;29(13):3111. doi:10.3390/molecules29133111.
59. Chu KH, Ali Hashim M, Hayder G. Boyd's film diffusion model for water contaminant adsorption: time for an upgrade? *J Mol Liq*. 2024;409:125466. doi:10.1016/j.molliq.2024.125466.
60. Wang L, Zhao Y, Sun M, Zheng Y, Fan H, Wang S, et al. Bifunctional sulfur-doped biochar for efficient removal of tetracycline and resistant bacteria via adsorption and peroxydisulfate activation. *Sep Purif Technol*. 2025;354(8):128728. doi:10.1016/j.seppur.2024.128728.
61. Zhu K, Shen Y, Hou J, Gao J, He D, Huang J, et al. One-step synthesis of nitrogen and sulfur co-doped mesoporous graphite-like carbon nanosheets as a bifunctional material for tetracycline removal via adsorption and catalytic degradation processes: performance and mechanism. *Chem Eng J*. 2021;412(7):128521. doi:10.1016/j.cej.2021.128521.
62. Xia S, Sun J, Sun W. Bimetallic metal-organic gel for effective removal of chlortetracycline hydrochloride from aqueous solution: adsorption isotherm, kinetic and mechanism studies. *Colloids Surf A Physicochem Eng Aspects*. 2022;649:129403. doi:10.1016/j.colsurfa.2022.129403.

63. Tran HN, Lima EC, Juang RS, Bollinger JC, Chao HP. Thermodynamic parameters of liquid-phase adsorption process calculated from different equilibrium constants related to adsorption isotherms: a comparison study. *J Environ Chem Eng.* 2021;9(6):106674. doi:10.1016/j.jece.2021.106674.
64. Wang W, Tian G, Zong L, Zhou Y, Kang Y, Wang Q, et al. From illite/smectite clay to mesoporous silicate adsorbent for efficient removal of chlortetracycline from water. *J Environ Sci.* 2017;51(4):31–43. doi:10.1016/j.jes.2016.09.008.
65. Zhang L, Tong L, Zhu P, Huang P, Tan Z, Qin F, et al. Adsorption of chlortetracycline onto biochar derived from corn cob and sugarcane bagasse. *Water Sci Technol.* 2018;78(5–6):1336–47. doi:10.2166/wst.2018.407.
66. Qin T, Wang Z, Xie X, Xie C, Zhu J, Li Y. A novel biochar derived from cauliflower (*Brassica oleracea* L.) roots could remove norfloxacin and chlortetracycline efficiently. *Water Sci Technol.* 2017;76(11–12):3307–18. doi:10.2166/wst.2017.494.
67. Chen X, Li H, Liu W, Meng Z, Wu Z, Wang G, et al. Low-temperature constructing N-doped graphite-like mesoporous structure biochar from furfural residue with urea for removal of chlortetracycline from wastewater and hydrothermal catalytic degradation mechanism. *Colloids Surf A Physicochem Eng Aspects.* 2020;600:124873. doi:10.1016/j.colsurfa.2020.124873.
68. Liu W, Sun J, Li X, Yuan K, Zuo S, Yao C, et al. Preparation of Ni Al hydrotalcite/clay/activated carbon and its adsorption of antibiotics in aqueous solution. *J Mater Sci Mater Electron.* 2022;33(36):26892–904. doi:10.1007/s10854-022-09354-8.
69. Song YX, Chen S, You N, Fan HT, Sun LN. Nanocomposites of zero-valent Iron@Activated carbon derived from corn stalk for adsorptive removal of tetracycline antibiotics. *Chemosphere.* 2020;255:126917. doi:10.1016/j.chemosphere.2020.126917.
70. Lv Y, Zhang R, Zeng S, Liu K, Huang S, Liu Y, et al. Removal of *p*-arsanilic acid by an amino-functionalized indium-based metal-organic framework: adsorption behavior and synergetic mechanism. *Chem Eng J.* 2018;339:359–68. doi:10.1016/j.ccej.2018.01.139.
71. Khamayseh MM, Kidak R. Equilibrium, kinetics, and thermodynamics study on the biosorption of reactive levofloxacin antibiotic on *Pithophora* macroalgae in aqueous solution. *Environ Monit Assess.* 2023;195(2):301. doi:10.1007/s10661-023-10925-3.
72. Nasseh N, Barikbin B, Taghavi L, Ali Nasser M. Adsorption of metronidazole antibiotic using a new magnetic nanocomposite from simulated wastewater (isotherm, kinetic and thermodynamic studies). *Compos Part B Eng.* 2019;159(8):146–56. doi:10.1016/j.compositesb.2018.09.034.
73. Salame II, Badosz TJ. Surface chemistry of activated carbons: combining the results of temperature-programmed desorption, boehm, and potentiometric titrations. *J Colloid Interface Sci.* 2001;240(1):252–8. doi:10.1006/jcis.2001.7596.
74. Zhang Y, Yu Y, Du G, Chen X, Zhao J, Jiang L, et al. Efficient removal of chlortetracycline hydrochloride by MOF-5-derived metal-free carbon materials with ultra-high specific surface area. *Colloids Surf A Physicochem Eng Aspects.* 2024;686(7):133474. doi:10.1016/j.colsurfa.2024.133474.
75. Filipkowska U, Jóźwiak T. Dye sorption from mixtures on chitosan sorbents. *Molecules.* 2024;29(15):3602. doi:10.3390/molecules29153602.
76. Chen Y, Liu J, Zeng Q, Liang Z, Ye X, Lv Y, et al. Preparation of *Eucommia ulmoides* lignin-based high-performance biochar containing sulfonic group: synergistic pyrolysis mechanism and tetracycline hydrochloride adsorption. *Bioresour Technol.* 2021;329:124856. doi:10.1016/j.biortech.2021.124856.